Enhanced refractor imaging by supervirtual interferometry

Ian Mallinson, King Abdullah University of Science and Technology and Imperial College London
Pawan Bharadwaj, King Abdullah University of Science and Technology and Indian School of Mines
Gerard Schuster, King Abdullah University of Science and Technology
Helmut Jakubowicz, Imperial College London

Refraction surveys are a well-established method of imaging subsurface velocities, both in terms of the deep crustal structure at global scales and in the shallow near surface. These surveys generally involve deploying an array of receivers on the surface (or water bottom) and recording arrivals from a seismic source initiated at or near the surface.

In an ideal case where an interface defines a boundary with a sharp increase in velocity, the head-wave refraction arrivals are described by raypaths which follow a diving-wave path down to the interface and refract along it, then follow a diving-wave path back to the surface (or water bottom) where the receivers are located. These arrivals, if they have a sufficiently high signal-to-noise ratio (SNR), are picked in the shot gathers and inverted to give the traveltime tomograms in either exploration-scale or global-scale tomography. However there are two common limitations of conventional refraction tomography:

1) Poor signal-noise ratio of first-arrival refractions at long offsets. Due to spherical divergence, attenuation and ambient noise, the SNR of head-wave refractions is insufficient for accurate picking of first-break traveltimes beyond a certain source-receiver offset.
2) Only first-arrival refractions are typically picked in the raw data, and "later" refraction arrivals are generally unpickable because of interference from body waves. As a result the maximum depth of investigation of refraction surveys is limited by the inability to identify later head-wave arrivals in the record.

Refraction interferometry offers the possibility of overcoming these limitations as it aligns and stacks together refraction arrivals that propagate along the same portion of the refractor (Dong et al., 2006). Similar to the NMO correction that flattens reflections in a CMP gather, interferometric correlation of traces recorded at two fixed geophones aligns the refraction arrivals from the same refractor; this alignment is valid for a large number of different source positions. The result is that head-wave arrivals generated from different sources can be stacked together to form virtual head-wave traces with an enhanced SNR (Bharadwaj and Schuster, 2010). This potentially offers a significant improvement over conventional processing of head-wave arrivals.

Theory

In a typical seismic experiment in a layered medium where the velocity increases with increasing depth, the first arrivals are generally refractions. In the case of head waves, these events have propagated along the interface between a low- and a high-velocity medium, and in the case of diving waves have been refracted upward along a curved raypath due to a velocity gradient. To consider a head wave as shown in Figure 1, its arrival at z can be approximated in the Fourier domain by:

$$u(w, z) = A(w, z)\, e^{i\omega(\tau_{wy'} + \tau_{y'z})} \quad (1)$$

and its arrival at y by:

$$u(w, y) = A(w, y)\, e^{i\omega(\tau_{wy'} + \tau_{y'y})} \quad (2)$$

where $\tau_{wy'}$ is the traveltime from w to y', $\tau_{y'z}$ is the traveltime from y' to z, $\tau_{y'y}$ is the traveltime from y' to y, and $A(w,y)$, $A(w,z)$ are amplitude terms which account for the source wavelet and geometrical spreading. As described by Dong et al. and Schuster (2009), the cross-correlation of these two events effectively generates a "virtual" head-wave refraction, with the source redatumed to lie on the refractor at point y' initiated at a time advance equal to $\tau_{y'y}$, as shown in Figure 1a:

$$\begin{aligned}\varphi(y, z)_w &= u(w, z)\, u(w, y)^* \\ &= |A(w, y)|\, |A(w, z)| e^{i\omega(\tau_{wy'} + \tau_{y'z} - \tau_{wy'} - \tau_{y'y})} \\ &\approx |A(w, y)|^2\, e^{i\omega(\tau_{y'z} - \tau_{y'y})} \end{aligned} \quad (3)$$

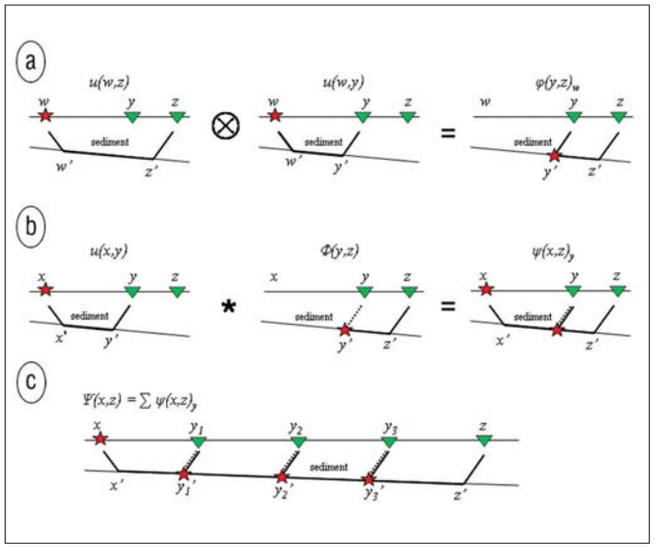

Figure 1.(a) *The source generating the head-wave arrival can be virtually redatumed to the refractor by correlating the traces recorded at* y *and* z*. The SNR can be enhanced by summing over many different postcritical source positions* w*. The dashed line indicates a negative traveltime. (b) The supervirtual head wave shown on the right can be generated by convolving the two events corresponding to the paths on the left, namely the recorded trace at* y *and the virtual trace at* z*. (c) By generating supervirtual traces for every position of* y *which lies between* x *and* z*, these traces can be summed to produce a stacked supervirtual trace with an improved SNR.*

Here $\tau_{y'z} - \tau_{y'y}$ is equal to the traveltime difference between a refraction arrival measured at y and at z for a source at w. For convenience the amplitude terms are assumed to be equal (i.e., A is independent of receiver position). Thus the cross-correlation yields an event which is equivalent to placing a source on the refractor at the point where the raypaths to y and z diverged. The signature for this source is now the autocorrelation of the original source signature, and it is initiated at a time advance of $\tau_{y'y}$.

A useful property of this result is that the redatumed event is now independent of the source position, provided the source is at a postcritical offset for this refractor. Thus, the correlated traces can be generated and summed for N shot positions to achieve an improvement in signal-to-noise ratio:

$$\Phi(y, z) = \sum_{w=1}^{N} \phi(y, z)_w \approx \sum_{w=1}^{N} |A(w, y)|^2 e^{i\omega(\tau_{y'z} - \tau_{y'y})} \quad (4)$$

From a physical perspective, this resulting function is equivalent to the trace measured at z for a shot on the refractor at position y', with the excitation time equal to $-\tau_{y'y}$. Due to the cross-correlation, Φ will also contain an acausal component at negative correlation lags which does not have a physical meaning.

It is important to note that there will be raypaths present in raw data which do not follow the path shown in Figure 1, such as reflections and diving waves. These will lead to unwanted artifacts in the cross-correlated traces which do not have a useful physical meaning. However, as these artifacts will occur at a different correlation lag for each shot, they will interfere destructively when the traces are summed. Conversely, the head-wave refractions will occur at the same correlation lag and so interfere constructively.

In order to remove the problems associated with the unknown time advance of the redatumed trace, it can then be convolved with a real trace recorded at y. This results in a second redatuming, generating a "supervirtual" head-wave refraction arrival at z for a source at x, as shown in Figure 1b:

$$\begin{aligned}\Psi(x, z)_y &= u(x, y)\, \Phi(y, z) \\ &= A(x, y)\, e^{i\omega(\tau_{xy'} + \tau_{y'y})} \sum_{w=1}^{N} |A(w, y)|^2 e^{i\omega(\tau_{y'z} - \tau_{y'y})} \\ &= A(x, y) \sum_{w=1}^{N} |A(w, y)|^2 e^{i\omega(\tau_{xy'} + \tau_{y'z})}\end{aligned} \quad (5)$$

This supervirtual head-wave arrival, $\Psi(x,z)_y$, is kinematically identical to what would be recorded by a geophone at z with a source at x. This process can be repeated for all M post-critical positions of y which lie between x and z, thus independently generating many traces for the same source and receiver positions. These traces can then be stacked to produce an output trace which has known surface source positions, and an enhanced SNR compared to a recorded trace, as shown in Figure 1c:

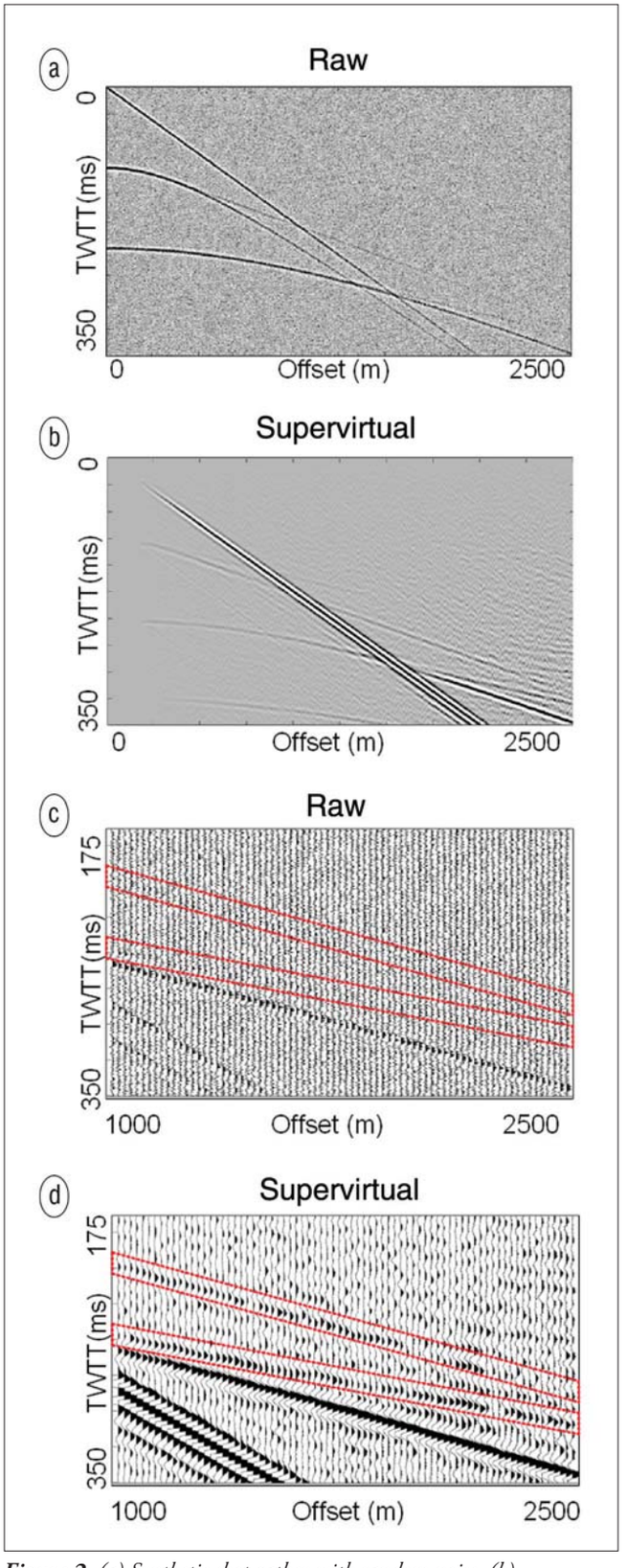

Figure 2. *(a) Synthetic shot gather with random noise. (b) Supervirtual shot gather showing improved SNR of refractions. (c) Wiggle plot of far offsets of raw data. (d) Wiggle plot of far offsets of supervirtual data.*

$$\Psi(x,z) = \sum_{y=1}^{M} \Psi(x,z)_y = \sum_{y=1}^{M} A\,|(x,y)| \sum_{w=1}^{N} |A\,(w,y)|^2 e^{i\omega(\tau_{xy'} - \tau_{y'z})} \quad (6)$$

where $\Psi(x,z)$ represents the stacked supervirtual trace. The SNR improvement in the stacked supervirtual trace compared to the raw trace is proportional to $\sqrt{M}$ (i.e., the number of supervirtual traces summed), if the effects of spherical divergence and discrete spatial sampling are ignored. For a given trace, M is the number of postcritical source/receiver positions which lie between the source and receiver for that trace, and so M increases with increasing offset. As a result, the SNR of supervirtual traces increases with increasing offset, while the opposite is true of raw traces.

Synthetic data example

Pressure traces are computed by ray tracing in a velocity model consisting of three flat, homogeneous layers. Each resulting shot gather contains a direct wave, a reflection from each interface, and a head-wave refraction from each interface, as shown in Figure 2a. The source and recording lines are along a horizontal surface; a Ricker wavelet with a peak frequency of 50 Hz is used as the source wavelet and the sampling interval is 1 ms. Random noise with a bandwidth of 5–100 Hz is added to all traces so that the refraction events are not clearly visible above the noise. Figure 2c shows the far offsets of the CSG after the addition of random noise; the reflections and direct wave are visible, but the head-wave refractions are masked by the noise. After application of the interferometry method described in the previous section, supervirtual traces are created and shown in Figure 2b as a CSG with an increased SNR, with Figure 2d showing an expanded view of the far offsets. Thus, first-arrival picking is possible for longer offsets than would otherwise have been possible. Note that the clarity of the supervirtual traces improves as offset (and hence M) increases. First-arrival traveltimes picked from the noise-free data and the supervirtual data agree to within 2 ms, well within the quarter period accuracy (5 ms in this example) required for traveltime tomography.

Field data example

Vertical component geophones are used to record refractions from a land survey over an area of Nevada consisting of poorly consolidated soil overlying bedrock. The shot and receiver intervals are 20 m and 5 m, respectively, and 102 shot records are recorded. Each shot record contains 240 traces, giving a total array length of 1200 m. A 5–100 Hz band-pass filter was applied to attenuate random noise in the data. A total of 24,480 traces were recorded during the experiment. A typical CSG with the band-pass filter applied is shown in Figure 3a, with an expanded view of the far offsets shown in Figure 3c. Traces with more than 800 m of source-receiver offset have very low SNR and so first-break traveltimes could not be picked for traveltime tomography.

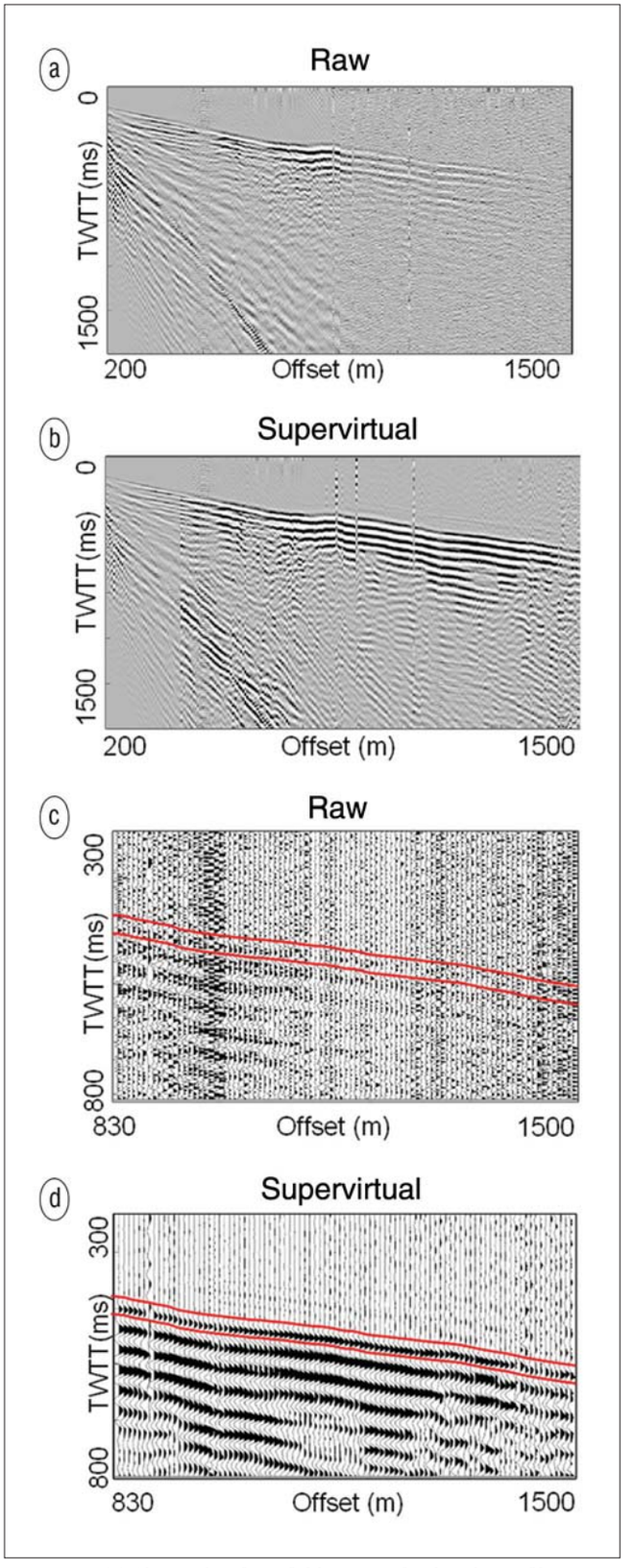

Figure 3. *(a) Shot gather from field survey after band-pass filtering. (b) Supervirtual shot gather showing improved SNR of bedrock refraction. (c) Wiggle plot of far offsets of raw data. (d) Wiggle plot of far offsets of supervirtual data.*

Figures 3b and 3d show the result of applying the supervirtual stacking method to the raw data. The SNR is increased considerably, allowing the first arrival to be picked all the way to the maximum offset. Figures 4a and 4b show the traveltime matrices resulting from picking all possible data in the filtered and supervirtual data, respectively. Only 68% of the total number of traces could be picked in the raw data, but this increased to 82% after supervirtual interferometry. Comparison of areas where both filtered and supervirtual first arrivals can be picked show that 95% of the supervirtual picks are within a quarter period of the corresponding picks from the filtered data, as shown by the histogram in Figure 4c. The largest errors are at very short offsets where the supervirtual method has very few source-receiver combinations to stack over, allowing wavelet irregularities to distort the result.

The picked first arrival traveltimes for both the filtered and supervirtual traces are inverted by the tomographic procedure described in Nemeth et al. (1997); the resulting tomograms are shown in Figure 5a and 5b. Because the actual velocity model is not known, it is not possible to say with certainty which result is correct, but the tomogram from the supervirtual data appear to show much improved resolution of the soil-bedrock interface near the left side of the image and does not contain the low-velocity zone which appears in the raw data tomogram.

Summary

We introduced a new refraction interferometry method that can be used to extend the aperture of refraction surveys by generating supervirtual traces with significantly higher SNR than the recorded traces. For well-sampled refraction surveys this means that refraction arrivals can now be picked over a greatly expanded aperture, thus improving the constraints on the subsurface velocity model in subsequent tomography. In the ideal case, the enhanced refractions can also be picked where they are not the first arrivals, and so allow the possibility of later-arrival refraction tomography. Initial tests with a field data set showed a potential improvement in the velocity tomogram compared to that obtained from the bandpass filtered raw data. Examination of the correlated traces can also help assess the head-wave or diving-wave nature of the refractor boundary. The potential drawback with this approach is that with coarsely sampled sources and a limited recording aperture, there will be artifacts due to the discrete approximation to the reciprocity equations. In this case, a least-squares approximation to the reciprocity equations could be used to mitigate such artifacts (Schuster and Zhou, 2006; Xue, 2009; Wapenaar et al., 2008).

In summary, supervirtual refraction interferometry can be a significant upgrade to refraction processing, resulting

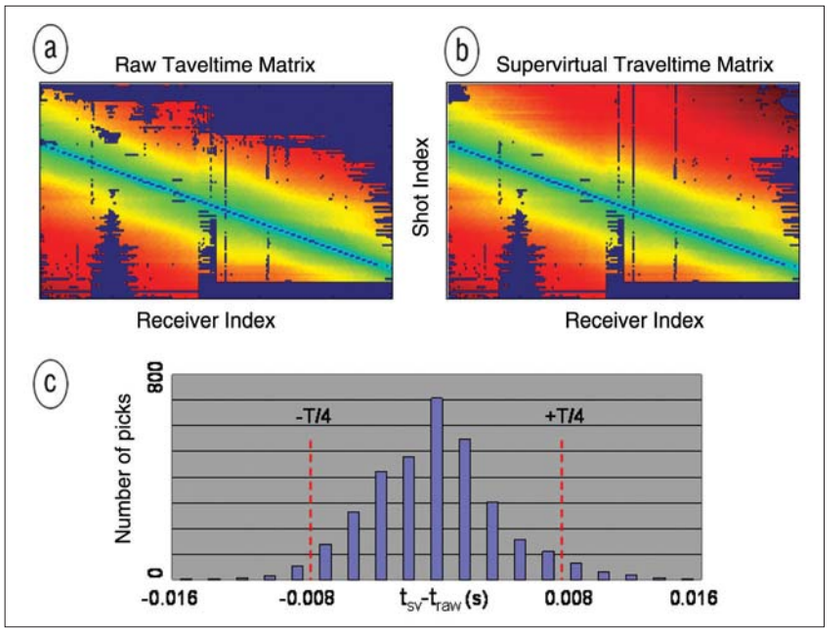

Figure 4. *(a) Traveltime matrix showing all possible picks from raw data. (b) Traveltime matrix showing all possible picks from supervirtual data. (c) Histogram comparing traveltime difference at traces where both raw and supervirtual data can be picked.*

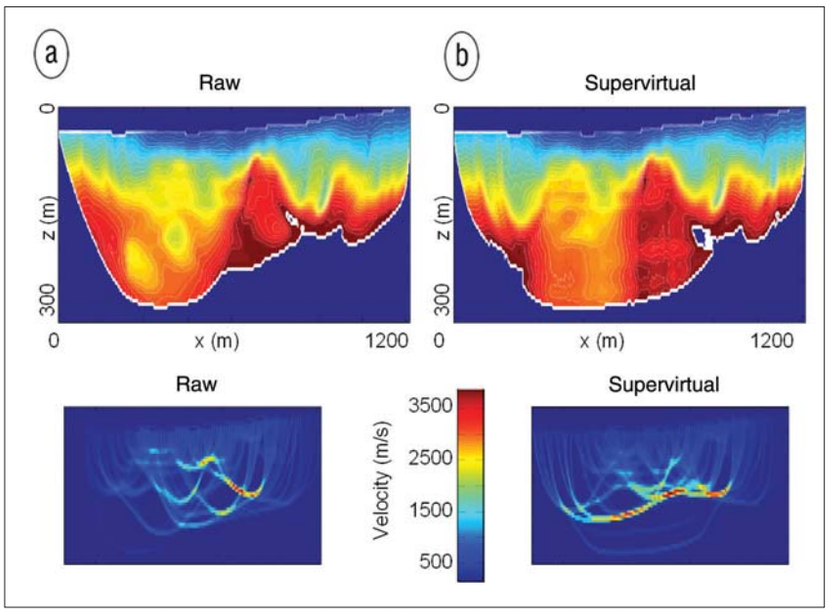

Figure 5. *(a) Velocity tomogram obtained from picks of raw data, showing poor resolution of the soil-bedrock interface on the left of the image. (b) Tomogram obtained from picks of supervirtual data, showing improved resolution of the interface.*

in a √M improvement in SNR. As M increases with increasing offset, the technique is most effective at far offsets where poor SNR is most problematical in raw data. This is similar in importance to that of stacking reflections after normal moveout, and can be applied at both exploration-scale and global-scale surveys. TLE

References

Bharadwaj, P. and G. T. Schuster, 2010, Extending the aperture and enhancing the S/N ratio of refraction imaging by super-virtual interferometry: Abstract S23C-04 presented at 2010 Fall Meeting, AGU

Dong, S., J. Sheng, and G. T Schuster, 2006, Theory and practice of refraction: 76th Annual International Meeting, SEG, Expanded Abstracts, 3021–3025.

Nemeth, T., E. Normark, and F. Qin, 1997, Dynamic smoothing in crosswell traveltime tomography: Geophysics, **62**, 168–176.

Schuster, G. T., 2009, Seismic interferometry: Cambridge University Press.

Schuster, G. T. and M. Zhou, 2006, A theoretical overview of model-based and correlation based redatuming methods: Geophysics, **71**, no. SI103–SI110, doi:10.1190/1.2208967.

Wapenaar, K., J. van der Neut, E. Ruigrok, D. Draganov, E. Slob, and J. Thorbecke, 2008, Seismic interferometry by cross-correlation or deconvolution?: 78th Annual International Meeting, SEG, Expanded Abstracts, 2731–2736, doi:10.1190/1.3063912.

Xue, Y., 2009, Least squares datuming and surface waves prediction with interferometry: Ph.D. dissertation, University of Utah.

Corresponding author: ianmallinson@hotmail.com